J Mater Sci: Mater Med (2011) 22:977–987
DOI 10.1007/s10856-011-4267-x

Surface characterization and biological response of carbon-coated oxygen-diffused titanium having different topographical surfaces

Osamu Yamamoto · Kelly Alvarez · Yuki Kashiwaya · Masayuki Fukuda

Received: 23 September 2010 / Accepted: 17 February 2011 / Published online: 2 March 2011

Abstract The materials (C-ODTi) with different topographical surfaces that possess interstitial oxygen atoms into the host titanium lattice and an upper nanometric surface layer of anatase-TiO_2 covered by a carbon thin layer were fabricated in this study. The carbon thin layer on the surface of C-ODTi was composed of amorphous carbon and nano-graphite crystals. In vitro tests, using human bone marrow-derived mesenchymal cells (hBMCs), were performed to check cytotoxicity, examining in particular cell morphology, cell proliferation, cell differentiation, and mineralization capability. After 10 days of culture a higher degree of cell viability was observed on the surface of C-ODTi with an abraded surface. We also observed that hBMCs cultured in direct contact with C-ODTi maintained their capability to express alkaline phosphatase activity (ALP) and formed mineralized nodules similar to the control cultures. Our results demonstrate that the carbon layer coating on the surface of C-ODTi possess better biological response than commercially pure titanium (cp Ti), which was evidenced by the higher proliferation rates of osteoblasts, higher osteo-differentiation and a higher mineralization capability.

O. Yamamoto (✉) · K. Alvarez · Y. Kashiwaya
Center for Geo-Environmental Science, Graduate School of Engineering and Resource Science, Akita University, 1-1 Tegata Gakuen-machi, Akita 010-8502, Japan
e-mail: yamamoto@cges.akita-u.ac.jp

M. Fukuda
Division of Dentistry and Oral Surgery, Akita University Hospital, 1-1-1 Hondo, Akita 010-8543, Japan

1 Introduction

The biggest challenge for the current biomaterials available for dental and orthopedic applications is making them induce rapid healing as well as controlled and guided bone growth around the implant leading to improved osseointegration [1]. A strong interfacial layer, with high mineralization potential, able to assure the biomechanical stability of the implant is also desired. The osseointegration process is complex and involves numerous factors in which the key role is played by topography and chemistry of the implant surface [2]. Modifying the surface of the implant either by changing the topographic features in the micrometer to nanometer range, or with a bioactive layer, or a combination of both, will enhance cell adhesion and proliferation and will increase osseointegration.

Numerous surface treatment modalities such as chemical treatment (acid and alkali treatment), electrochemical treatment (anodic oxidation), sol–gel, chemical vapor deposition (CVD), physical vapor deposition (PVD), plasma-spray deposition, ion implantation, thermal oxidation, etc. have been employed to improve the quantity and quality of bone bonding and to develop a multi-functional implant surface by changing the composition, thickness, porosity, crystallinity and surface morphology of the titanium layer which is passive against bioactivity [3–11]. The formation of the crystalline oxide layer based on thermal oxidation treatment of titanium is a low cost and simple process that can be readily applied to modify the external surface of metals without changing the core or the shape of the implants, which has lead to enhanced bone formation around dental implants after functional loading [12, 13].

In the current investigation, a newly developed material called carbon-coated oxygen-diffused titanium, i.e., C-ODTi, has been fabricated by means of a especial thermal oxidation

treatment, where the chemical analyses of the surface structure and the biomimetic characteristic on the fabricated C-ODTi have been described [14]. In the C-ODTi, the surface of titanium has been modified where the top 20 nm consists of amorphous carbon layer and the subsequent upper 140 nm consists of anatase-TiO_2 layer. Here, the material exhibits a diffusion layer; which consists of a continuous layer of about 240 nm of α-Ti, rich in interstitial oxygen atoms and from that is the material's name. Since clinical and experimental data have shown that roughened surfaces allow successful osseointegration, we have also made a topographical modification by applying a mechanical grinding treatment to the surface of the fabricated C-ODTi.

This study builds upon our previous work, which showed that C-ODTi exhibits biomimetic properties. Given that osteoblasts are responsible for producing the mineralized extracellular matrix of bone, the assessment of the osteoblast response when the cells are in direct contact with a biomaterial is necessary. In the present study, we have focused on evaluating in vitro cell proliferation, osteogenic differentiation and mineralization capability of hBMCs cultured directly on the C-ODTi surface for several weeks.

2 Materials and methods

2.1 C-ODTi fabrication

Four different surface treatments were investigated in this study, which were indicated using the following abbreviations:

(A) cp Ti group
1. S sample: cp Ti disks with smooth surfaces
2. R sample: cp Ti disks with abraded surfaces

(B) C-ODTi group
3. SO sample: C-ODTi disks with smooth surfaces
4. RO sample: C-ODTi disks with abraded surfaces

For the preparation of the SO and RO samples we followed the procedure shown in Fig. 1. Briefly, S and R samples were cleaned ultrasonically in pure acetone, ethanol and distilled water for 20 min followed by immersion into a 20 wt% aqueous solution of poly(vinyl alcohol) (PVA#2000, average molecular weight $M = 88$ kg/mol, 72–82 mol%, hydrolyzed, Kanto Chemical Co. Inc., Tokyo, Japan). The PVA-coated S and R samples were allowed to dry on a glass plate at 70°C for 24 h. Subsequently, the samples were thermally treated at 700°C for 1 h in an argon (99.999%) atmosphere. The flow rate of argon gas was 50 cm^3/min. Before the thermal treatment, the furnace was filled with argon gas at a flow rate of 100 cm^3/min for 90 min. Before use the disks were placed on a sterile watch glass and were dry-heat sterilized at 180°C for 2 h. The S sample was used in the "as-received" condition. The R and RO samples were prepared by means of a mechanical grinding treatment, which is explained in more detail in the next section.

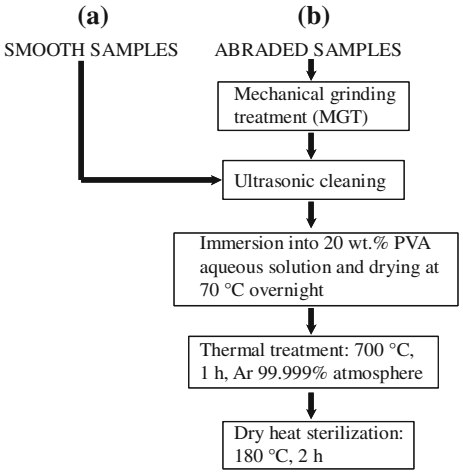

Fig. 1 Schematic diagram of the fabrication procedure of the C-ODTi. (*a*) SO sample, and (*b*) RO sample

2.2 Abrasion treatment of titanium specimens

Round disks (∅ 10 mm, 0.5 mm thick) of cp Ti metal (Ti > 99.9%) (Nilaco Co., Tokyo, Japan) were abraded with an electric micro grinding machine (Urawa Manufacturing Co. Ltd., Saitama, Japan). This mechanical grinding treatment (MGT) of the titanium surface was carried out in order to generate a certain surface roughness and consequently improve the cell adhesion and proliferation. The MGT was conducted at room temperature without coolant, abrading the samples by means of a resin-bonded silica sand wheel rotating at 3.35 m/s (8000 rpm). Following the MGT, the samples were washed with pure acetone, ethanol and distilled water in an ultrasonic cleaner.

2.3 Surface characterization

The surfaces of the samples were examined before the analysis using a field-emission scanning electron microscope (FE-SEM; HITACHI S-4500, Japan). The phases and the crystal structure of the fabricated material were identified by thin film X-ray diffraction (TF-XRD; RINT 2000, Rigaku Co., Tokyo, Japan) using Cu K_α radiation at 40 kV and 40 mA power. Data were recorded over the range $\theta = 20°–60°$ with a step size of 0.02° and step duration of 0.4 s. The properties of the carbon layer coating on the C-ODTi surface were investigated using laser

Raman spectroscopy. Raman spectra were obtained at room temperature using the backscattering method, by spectroscope (JASCO NRS-3100, Japan) with an air-cooled CCD detector. A green laser with an excitation wavelength of 532.07 nm was used. The excitation energy and area were 10 mW and 1 μm, respectively. Backscattered Raman signals were collected and recorded from 1000 to 1800 cm^{-1} with a lateral resolution of 1 cm^{-1}. The band fitting of the first order Raman spectra was performed using Lorentzian and Gaussian functions based on a straight baseline within 1000–1800 cm^{-1}.

The surface roughness of the samples was measured by profilometry using a SURFCOM 3000A (Tokyo Seimitsu Co. Ltd., Japan). Average surface roughness (R_a) and peak-to-valley height (R_z) measurements were taken at three different points on each type of sample to obtain an average value and a standard deviation.

The C-ODTi surface morphologies and their roughness were evaluated by atomic force microscopy (AFM: NPX 100M001 Seiko Instruments Inc., Japan). The microscope features a NPX 100 microscope unit controlled by a Nanopics 1000 controller (Seiko Instruments Inc., Japan) and was operated in a dynamic force mode with a self-sensing cantilever (force constant at 30 N/m and a resonance frequency of 300 kHz). Wide-range images of 150 μm × 150 μm were collected as constant force images (i.e., height mode images) in x–y scan range and 3 μm in z range. The average roughness represented by the root mean square (RMS) roughness of the surface (which is the standard deviation of the mean z values) was calculated based on a standard formula integrated in the software. A line profile of 200 μm was taken from each sample to calculate the RMS of the samples.

2.4 In vitro biocompatibility assays

2.4.1 Cell culture

Healthy hBMCs were isolated from bone marrow aspirates, after informed consent, from a newborn baby donor via density gradient centrifugation [15]. Tissue was used with the approval of Akita University Research Ethics Committee. The cells were expanded in Eagle minimum essential medium (α-MEM; Sigma, M8042) supplemented with 10% fetal bovine serum (FBS; CELLect GOLD, ICN Biomedicals Inc.) and 1% penicillin/streptomycin (Gibco, Invitrogen Co.) at 37°C in a humidified atmosphere where 5% of the air was CO_2 and subcultured every 7 days. The medium was completely renewed every third day. The passages of 4–9 times were performed in the experiments. In all the experiments, control cells were grown on a polystyrene cell culture dish (Costar, Cambridge, MA) in the absence of test materials.

2.4.2 Cell morphology: crystal violet staining

After different culture periods, the supernatants of the 48-well plates were discarded and the cell monolayer was rinsed twice with 300 μl of phosphate-buffered saline (PBS) consisting of 137 mmol/l NaCl; 2.7 mmol/l KCl; 4.3 mmol/l Na_2HPO_4; 1.47 mmol/l KH_2PO_4 and subsequently fixed with 10% phosphate buffered formalin solution. Fixed cells were incubated in 0.2% crystal violet in a 2% ethanol solution (Wako Pure Chemical Industries, Ltd.) for 10 min at room temperature. The excess dye was removed by three rinses with distilled water. The plates were the air dried overnight and observed with an optical microscope.

2.4.3 Cell viability: MTT assay

Viability of the hBMCs was determined by means of MTT assay. Cells were seeded onto dry-heated sterilized cp Ti and C-ODTi that perfectly fit the bottom of the wells of a 48-well cell culture dish. Cells were seeded onto the discs at a density of 5×10^3 cells per well and incubated for 1, 4, 7, and 10 days. Changes in the number of the viable cells on the substrates were quantitatively assessed by MTT-based colorimetric assay [16]. Thirty microliters of tetrazolium salt solution, 3-[4,5-dimethyl-2-thiazolyl]-2,5-diphenyltetrazolium bromide (MTT) (Dojindo Laboratories, Kumamoto, Japan) (600 mg/l in cell culture medium), was added to each well. After incubation for 4 h at 37°C, the MTT solution in the medium was removed. The incorporated formazan crystals in the cells were solubilized with 300 μl of dimethylsulfoxide. The absorbance of each well was then read at 570 nm using a 96-well microplate reader (Multiskan JX; THERMO Electron Co., Helsinki, Finland) equipped with Ascent version 2.6 microplate analysis software (Labsystems, Waltham, MA, USA). A standard curve of known viable cells numbers was used to calculate viable cell numbers for the different time points.

2.4.4 Alkaline phosphatase activity (ALP)

hBMCs were put in a 48-well cell culture dish at a density of 5×10^3 cells per well and cultured for 2, 5, 7, 14, 21 and 28 days. The medium was replaced on days 5, 8, 12, 15, 19, 22 and 26. After each culture time, the cell layers were washed twice with 300 μl of PBS. A substrate, p-nitrophenylphosphate Disodium (Wako Pure Chemical Industries LabAssay™ ALP, 1 tablet) was dissolved in a substrate buffer (0.1 mol/l Carbonate buffer, pH 9.8, 2.0 mmol/l $MgCl_2$) (5.0 ml), and 250 μl of this solution was added to each 48-well plate directly onto the monolayer. The plates were incubated at 37°C for 20 min.

The reaction was stopped by adding 200 µl of 0.05 mol/l NaOH. The amount of released *p*-nitrophenol (pNP) was measured at 405 nm in a 96-well microplate reader. Enzyme activity was calculated using calibration curves and was expressed as a concentration of pNP in 20 min/10^6 cells. A minimum of two samples were assayed at each time point and values were normalized by the number of cells at each time point determined by the crystal violet assay [17].

2.4.5 Mineralization assay

Mineralization was induced in confluent monolayers after 7 days of culture in ordinary medium. The cells were plated at a concentration of 5×10^3 cells per well in a 48-well cell culture dish. The primary ordinary medium was replenished on day 4. On day 7, the cells were provided with a secondary osteogenic medium consisting of α-MEM supplemented with 15% fetal bovine serum (FBS; CELLect GOLD, ICN Biomedicals Inc.) and 1% penicillin/streptomycin (Gibco, Invitrogen Co.), 10 mM β-glycerophosphate (Sigma-Aldrich), 0.28 mmol/l ascorbic acid 2-phosphate (Wako Pure Chemical) and 100 nmol/l dexamethashone (Sigma-Aldrich) [18]. The osteogenic medium was renewed twice a week and the cultures were maintained up to 28 days. Materials samples incubated in the absence of cells were used as a negative control.

At the end of the culture period, the monolayers in the 48-well dishes were washed with PBS solution, and then were fixed for 15 min with 300 µl of a 10% cold neutral phosphate buffered formalin solution. The monolayers were then rinsed three times with distilled water prior to the addition of 300 µl of 40 mmol/l Alizarin red S (pH 4.1) solution. The plates were incubated at room temperature for 10 min and then washed well with distilled water. Nodules were visualized by using an inverted microscope for the control samples and a metallographic microscope for the metallic samples. The stain was solubilized for 30 min at room temperature with 0.5 mol/l HCl-5% sodium dodecyl sulphate (SDS). Then, 100 µl of the solubilized stain was moved to a 96-well cell culture dish where the absorbance was measured at 405 nm using a microplate reader.

Some cultures were prepared for observation in the FE-SEM equipped with an energy dispersive X-ray spectrometer (EDX). The cultures were fixed with 4% formaldehyde in a 0.1 mol/l PBS solution, baked in a furnace at 180°C for 60 min for dehydrating, and then furnace cooled to room temperature, and finally coated with a thin layer of carbon. The evaluation of mineralization consisted of a morphological and compositional examination of the calcified mineral formed using EDX.

2.5 Statistical analysis

Each experiment was repeated at least three times with similar results. Results are expressed as a mean ± standard deviation (SD). Error bars in the figures represent standard deviations. The cell proliferation and differentiation data were analyzed by a Student's *t*-test for statistical significance, and P values < 0.05 were considered significant. Statistical analysis among the groups was performed by the ANOVA test. The Tukey test was used for all *post hoc* multiple comparisons.

3 Results

3.1 Effects of surface treatment

3.1.1 Effect of the surface chemistry

Figure 2 shows the TF-XRD pattern of the surface of SO sample. Single anatase-TiO_2 phase was found in the outermost surface. No carbon diffraction peaks were detected. It can be inferred that the carbon residues generated due to the thermal decomposition of the PVA are amorphous in a result of the TF-XRD. The results of X-ray photoelectron spectroscopy (XPS; Perkin–Elmer ESCA 5600, USA) have been presented and discussed in detail elsewhere [14] but will be summarized simply here to better describe the characteristics of the C-ODTi. Comparison of the chemical composition of the pure titanium and oxygen-diffused titanium surfaces by XPS revealed that the surface concentrations of oxygen and carbon were higher in the latter material. In the C-ODTi the relatively high carbon concentration was a product of the thermal decomposition of the polyvinyl alcohol coating that was applied on the material before the heat treatment at 700°C. The nature of this carbon surface

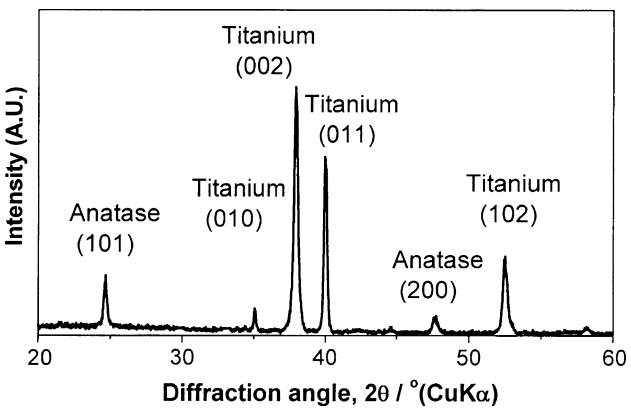

Fig. 2 TF-XRD pattern of the surface of the SO sample fabricated by heat-treatment of a PVA-coated Ti plate in an argon (99.999%) atmosphere for 1 h

layer seemed to be amorphous pyrocarbon. On the other hand, C-ODTi exhibited a single anatase-TiO_2 layer and a α-Ti–O diffusion zone below the amorphous carbon layer. These results described above were the same on the surfaces of the C-ODTi both with and without abrasion, i.e., SO and RO samples. Though the carbon layer on the C-ODTi surface was amorphous in TF-XRD and XPS measurements, it is inadequate to make sure what the carbon is really amorphous. In such cases, Raman spectroscopy has been used to examine carbon materials of amorphous and graphitic structures, because two large peaks around 1350 and 1580 cm^{-1} can be attributed to the D-band originating from the disordered structure and the G-band assigned to the graphite-like structure, respectively [19–21].

Raman spectra of the carbon layer formed on the surface of SO sample are shown in Fig. 3, together with that of the S sample. None of the Raman peaks were detected in the S sample, whereas two large peaks at about 1350 and 1615 cm^{-1} were observed in the SO sample. The band fitting was performed on the observed two peaks, and five peaks appeared at 1280, 1350, 1500, 1580 and 1615 cm^{-1}. A broad peak at 1280 cm^{-1} may be the spectrum assigned to the C–H vibration on the carbonaceous matrices produced by the pyrolysis of PVA, which accorded with the results reported by Goto, et al. [22]. A peak at 1500 cm^{-1} can be attributed to D″-band assigned to an amorphous form of sp^2 carbon, and a D′-band originating from the disordered structure appeared at 1615 cm^{-1} as well. These results were almost in agreement with the detailed Raman results of pyrocarbon reported by Vallerot et al. [23]. The in-plane size of graphite crystals, L_a, in nanometers, can be calculated by using the following Eq. 1 [24]:

$$L_a \fallingdotseq 4.4(I_G/I_D) \quad (1)$$

where I_G and I_D are the intensity of the G- and D-bands, respectively. The in-plane size of graphite crystals was about 3.7 nm. The carbon layer on the surface of SO sample is anticipated to compose of amorphous carbon and nano-graphite crystals. The above-mentioned Raman spectroscopy results were identical to those on the RO sample, i.e., there was no difference between SO and RO sample.

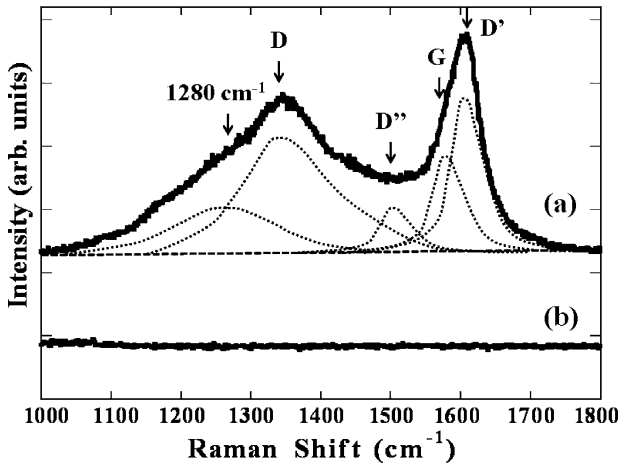

Fig. 3 Raman spectra of the surface of (*a*) SO and (*b*) S samples

3.1.2 *Effect of the surface topography*

Figure 4a and b show the topographical features of the surface of C-ODTi, observed by AFM. The abrasion treatment increased the surface roughness on a micrometer scale in the SO and RO samples. The AFM scans on the surface assessed a RMS roughness value of 1.29 and 2.43 μm, for the SO and RO samples, respectively. In Fig. 4b many grinding grooves were observed and no Si contamination on the grinded surfaces was detected by EDX. The change in the average profilometry surface roughness before and after the mechanical and chemical surface modification can be observed in Fig. 5. The S sample exhibited the lowest average roughness, whereas the RO sample showed the highest values. The SO and RO samples roughened after the thermal treatment, probably due to the growth of an oxide film and carbon deposition originating from the PVA decomposition that occurs around 250°C.

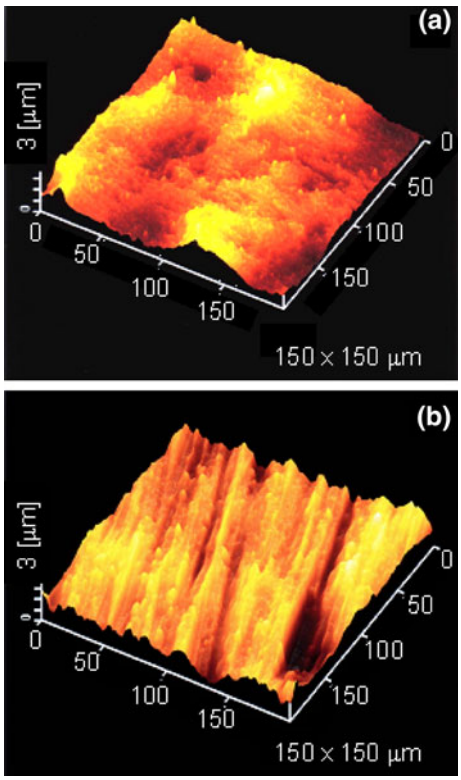

Fig. 4 AFM images of **a** SO and **b** RO samples. RMS values were 1.29 and 2.43 μm, for the smooth and abraded surfaces, respectively

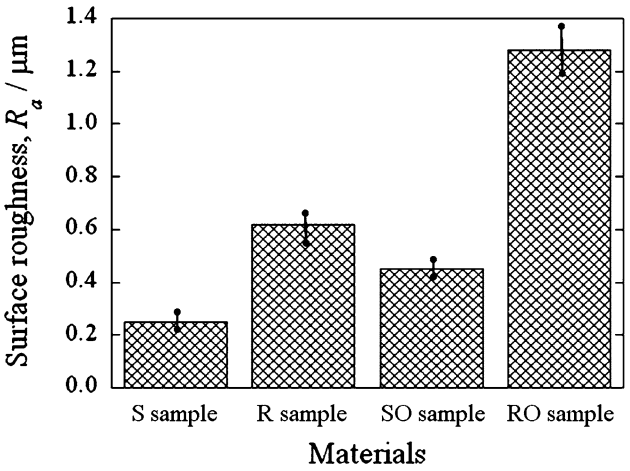

Fig. 5 Roughness of the samples in this study: S sample, R sample, SO sample, RO sample

3.2 In vitro biocompatibility evaluation

3.2.1 Cell morphology

After staining with crystal violet the cell morphology was examined by optical microscope (OM). Figure 6 shows the typical features of the cells after 3 days of culture directly on the evaluated materials. In all the tested surfaces, spreading polygonal-shaped cells were observed. No differences in either cell size or morphology were detected after culturing the human osteoblasts on the C-ODTi up to 28 days. As can be seen in the optical images of Fig. 6, the cells cultured directly on each sample spread out on all the samples and looked flattened and well attached without significant morphological changes in comparison with the control cells cultured on the plastic cell culture dish.

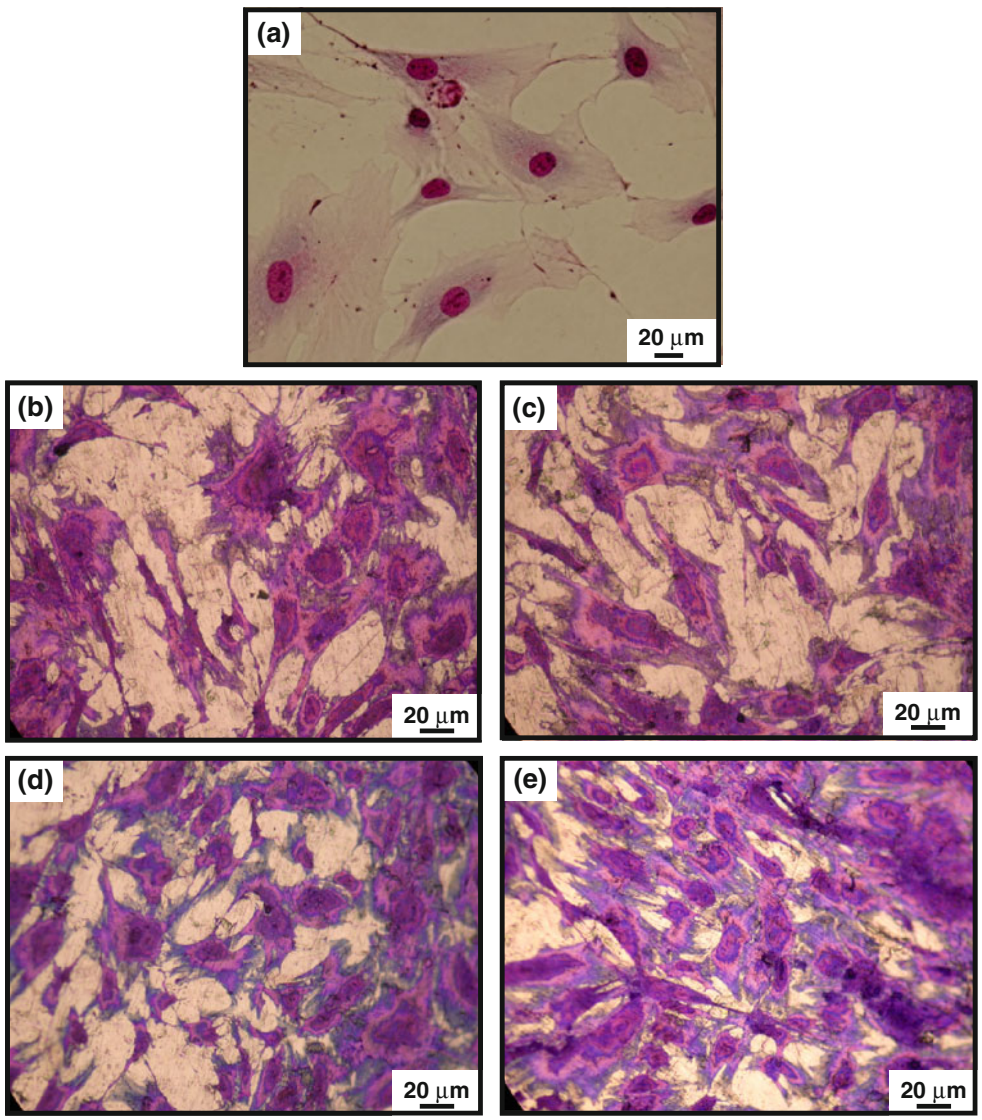

Fig. 6 Optical microscope images of the hBMCs cells directly cultured on the samples after 3 days of culture. **a** cell culture dish; **b** S sample; **c** R sample; **d** SO sample; **e** RO sample. The cells demonstrated normal morphology on all surfaces. Images at 400× magnification

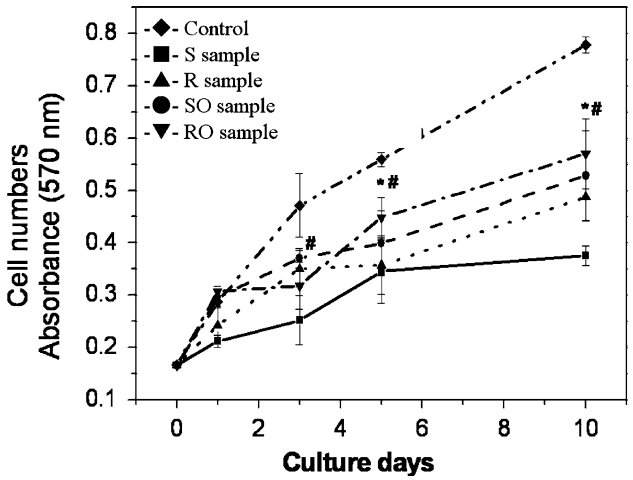

Fig. 7 Cell proliferation measured by the MTT test. MTT activity was determined as indicated in the section of material and methods. Data are expressed as the mean values ± SD of three experiments. As control cells without any material were cultured and analyzed. There were significant differences between the control and the samples ($*P < 0.05$); $^{\#}P < 0.05$ versus the S sample

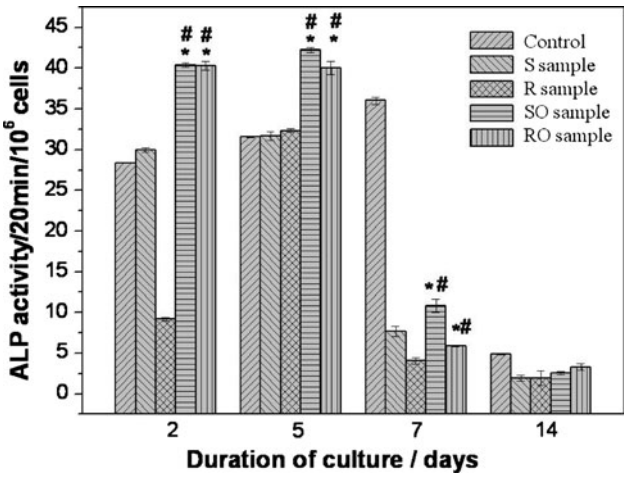

Fig. 8 ALP activity expressed by hBMCs cells on each sample after culturing up to 14 days. Polystyrene cell culture dish was used as a control. *Bars* represent the mean value of three experiments; *brackets* represent SD. There were significant differences between the control and the samples ($*P < 0.05$); $^{\#}P < 0.05$ versus the S sample

3.2.2 Cell viability: MTT assay

Figure 7 shows the results of the MTT proliferation assay. The number of metabolically active cells on the material's surfaces were measured over different periods (1, 3, 5 and 10 days) and it was observed that although the osteoblasts proliferation resulted to be smaller than the control, osteoblasts cultured on RO sample showed significantly higher cell numbers than on S sample. In general it was observed that in the surfaces of R, SO and RO samples, the cell numbers were higher.

3.2.3 ALP activity

To examine cell differentiation, the ALP was measured as a marker of osteoblasts differentiation. The expression of ALP is needed before matrix mineralization. It provides localized enrichment of inorganic phosphate, one of the components of the mineral phase of bone [25]. Figure 8 shows the results of the ALP tests performed on the evaluated materials. In this study, the ALP was expressed related to the cell number, eliminating the effect of proliferation in this parameter. The cells cultured on the plastic cell culture dish (control) exhibited a maximum in ALP activity after 7 days in culture. In the both samples of cp Ti and C-ODTi, this maximum was observed on the fifth day of culture and then significantly decreased on the seventh day. In comparison with the control and the cp Ti surfaces, the surface of C-ODTi showed higher ALP activity during the first 5 days of culture. At day 14 the cells cultured on the C-ODTi surfaces showed higher ALP activities than those on the cp Ti surfaces and the obtained values were very similar to the ALP activity of the control culture. ALP plays a crucial role in the initiation of matrix mineralization, and following that expression, this enzyme is down-regulated in the early stages of the mineralization [26, 27]. This fact explains the decline in the ALP activity observed on day 7 and day 14 of the culture.

3.2.4 Mineralization assay

In culture, hBMCs have the ability to form bone-like structures [28], for this reason bone marrow cell cultures are recommended to screen biomaterials on their osteoinductive capacity [29]. Bone nodule formation was observed using Alizarin red staining. Alizarin red is a calcium-sensitive dye used to identify tissues highly rich in hydroxyapatite [30, 31]. Osteoblast cells developed calcified nodules, i.e., red-stained portion, after 28 days of culture in the presence of osteogenic medium. It was observed that the density and distribution of the calcified nodules varied according to the material surface. On the C-ODTi circular-shaped nodules were evenly distributed across the whole surface which was very similar to the control cultures. While on the cp Ti the nodules were found in some areas but not over the whole surface.

Figure 9 shows the extent of calcium deposition on the fabricated materials, after incubation in an osteogenic cell culture medium for 28 days. The amount of calcium deposition was determined quantitatively by dissolving the nodules in a diluted chloridric acid solution and reading the absorbance at 405 nm. The results demonstrated that the RO sample exhibited significantly elevated levels of mineral nodule formation, very similar to the control

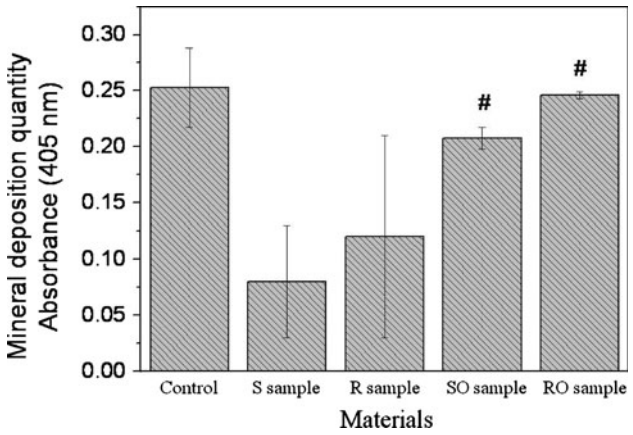

Fig. 9 Extent of bone-like nodule formation after 28 days of direct culture on each sample. Cultures were fixed and stained with alizarin red, which was solubilized with 0.5 mol/l HCl-5% SDS. Data are expressed as the mean values ± SD of three experiments. $^{\#}P < 0.05$ as compared to S sample

group. Compared to the cp Ti, C-ODTi was significantly better at promoting the mineralization in the human osteoblasts culture.

To confirm that the in vitro mineralization observed represents bone formation, the mineral nodules formed were examined by EDX elemental analysis of the surface, and element distribution maps for Ca and P were also made. EDX punctual analysis, made directly on the calcified biological structures found on the surface of SO sample, confirmed the presence of Ca, P, and O, characteristic elements of osteogenic tissue (Fig. 10b). Minor traces of Na, Mg and S (due to the alizarin red staining) were also detected. The Ca/P ratio of the nodules was 1.32, which is close to the value of the Ca/P of the rabbit bone used in the in vivo experiments (1.58). Figure 10c and d show the results of the chemical mapping obtained by EDX on the SO sample showing the distribution of Ca and P in the calcified nodules, respectively. The morphology of the globular deposits indicates that the mineralization was produced by the hBMCs. The bone-like nodules consisted of a fibrillar extracellular matrix (ECM) and the appearance was similar to the previously reported bone-like nodules formed by bone marrow cells when cultured directly on biomaterials [32].

4 Discussion

4.1 Effects of surface treatment

4.1.1 Effect of the surface chemistry

Surface modification on titanium can alter the surface topography and chemistry, which directly affect the biological reaction to implants; that is, the interaction between

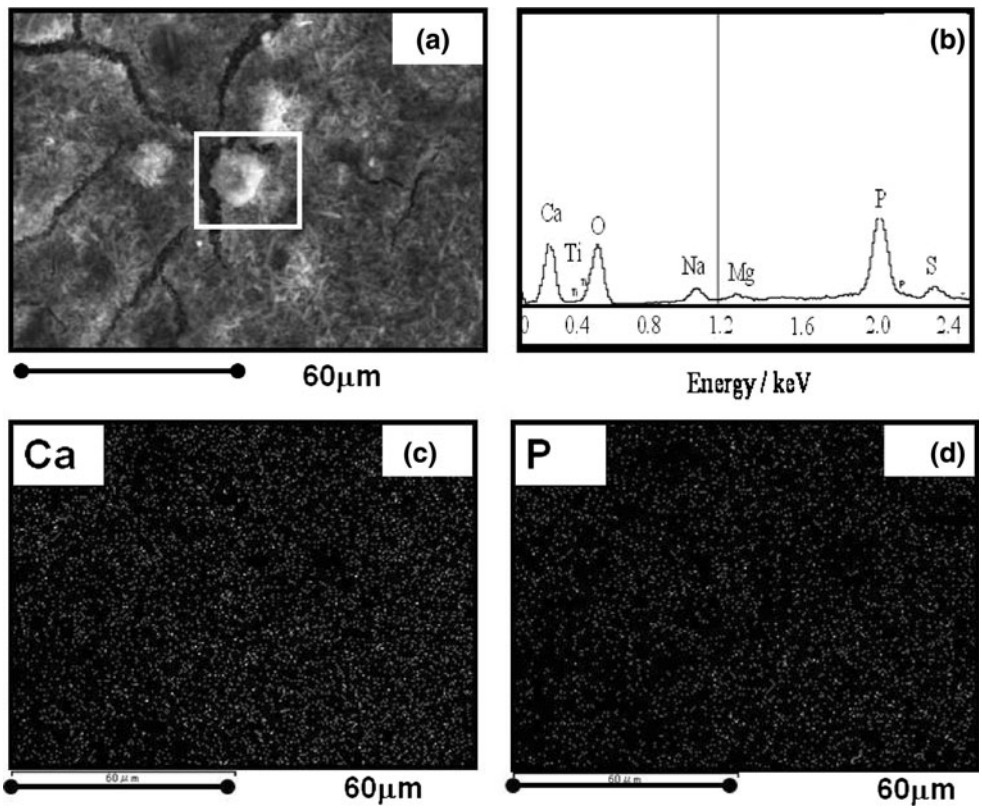

Fig. 10 **a** FE-SEM image showing the mineral nodules formed after the mineralization assay after 28 days of incubation on the surface of SO sample; **b** EDX microanalysis performed on the squared area of the SO sample; **c** EDX image mapping showing the location of Ca element on the surface of SO sample; **d** EDX image mapping showing the location of P element on the surface of SO sample

implants and biological environments. From previously performed XPS analyses [14] it is assumed that C-ODTi has a surface compound layer formed entirely of a TiO_2 anatase structure covered by an amorphous carbon layer. From laser Raman spectroscopy, however, it is revealed in this study that the carbon layer on the surface of C-ODTi sample was composed of amorphous carbon and nano-graphite crystals. For the C-ODTi, the total thickness of the surface oxide layer is about 400 nm and has a concentration gradient of oxygen long the depth due to the presence of an oxygen diffusion zone [14].

The carbon thin layer on the C-ODTi surface seems to be suitable for implant applications since no cytotoxic effect to the hBMCs was found. Additionally, the cells were able to proliferate, synthesize a cellular matrix, express the enzyme alkaline phosphatase, which is related to bone differentiation and show mineralization in the form of a calcium–phosphate material.

4.1.2 Effect of the surface topography

SEM indicated that topographical changes resulted from the abrasion treatment applied, and this influenced the observed in vitro and in vivo cell responses. Several researches have shown that osteoblastic proliferation could be enhanced by rough surfaces [33–35]. It is also known that cell responses to titanium surface characteristics have been shown to vary with cell types as well as cell maturation states [36, 37]. However, from in vitro to in vivo studies, a common agreement that greater initial cell attachment of osteoblasts on rough surfaces on titanium occurs as long as the degree of roughness is within the dimension of individual cells [34, 38]. For example, Bowers et al. [34] demonstrated that in rat calvarial cells cultured on titanium surfaces in the range of R_a from 0.14 to 1.15 μm, the maximal attachment was obtained on the surfaces with a R_a of 0.87 μm. The effect of surface roughness on cell adhesion probably results from the fact that rough surfaces may adsorb more fibronectin than smooth surfaces [39]. Fibronectin is a cell adhesion protein present in serum, which can mediate cell attachment when spread on artificial substrates by interacting with glycosaminoglycans and the cytoskeleton [40], preserving the synthesis of extracellular matrix proteins [35].

4.2 In vitro biocompatibility evaluation

4.2.1 Cell morphology and cell viability by MTT assay

Microscopic observations revealed that cell distribution and morphology on the surfaces of the materials was regular and normal. Although all the evaluated materials showed a continuous cell layer formation, significantly reduced cell proliferation and cell numbers were found on the cp Ti, showing that osteoblasts cells directly cultured on the C-ODTi had a better biological response. Also, the cell proliferation observed on the smooth surfaces was smaller than on the rough surfaces. In the present study, the roughness values were in micrometric range and this range (roughness at the cellular scale) is believed to be the ideal range to influence the adhesion and proliferation of the cells [41].

4.2.2 ALP activity and mineralization

Compared with the cp Ti and culture dish, increased ALP activity was found on the C-ODTi indicating that the osteoblasts differentiation process was not inhibited due to toxic material effects. On the contrary, C-ODTi surfaces may contribute to osteogenic differentiation. The elevated ALP activity levels of these samples indicate that higher numbers of differentiated cells were present and this results correlates well with mineralization capability. The increased ALP activity found on the C-ODTi resulted in more bone-like nodule formation as shown in Fig. 7. In a previous study [14] C-ODTi was subjected, in vitro, to a bioactivity test and on the mineral deposits were precipitated at the surface of C-ODTi, showing that the C-ODTi surface is bioactive. The results of the mineralization assay using hBMCs confirm the fact that C-ODTi promotes the formation of minerals containing Ca and P. This property is very important since it determines the capacity of the material to allow in vivo bone ingrowth on its surface.

5 Conclusions

C-ODTi was fabricated to increase the cellular biocompatibility of titanium. Surface characterizations have shown distinct differences in the topography of the fabricated materials. According to the biological tests the chemical composition of the external surface, i.e., carbon layer, of C-ODTi resulted in being non cytotoxic. When human osteoblasts were cultured directly on C-ODTi normal cell morphology and proliferation as well as higher cell numbers than in cp Ti were obtained. The results showed high ALP activity and the presence of mineralized bone-like nodules on C-ODTi, suggesting that the fabricated material does not impair the differentiation and mineralization process of the osteoblasts cells. Therefore, C-ODTi with an anatase outermost surface covered by a nanometric carbon layer plus a layer of interstitially diffused oxygen beneficially affected the surface improving its biocompatibility. In summary, the present study showed that a dual mechanical and chemical treatment of implants increased the in vitro biocompatibility

of titanium. The C-ODTi appears to be a promising biomaterial capable of accelerating the bone formation and improving the osseointegration in cortical bone implants.

References

1. Brunski JB, Puleo DA, Nanci A. Biomaterials and biomechanics of oral and maxillofacial implants: current status and future developments. Int J Oral Maxillofac Implants. 2000;15:15–45.
2. Wenneberg A, Albrektsson T, Johansson C, Anderson B. Experimental study of turned and grit-blasted screw-shaped implants with special emphasis on effect of blasting material and surface topography. Biomaterials. 1996;17:15–22.
3. Sittig C, Textor M, Spencer ND, Wieland M, Vallotton PH. Surface characterization of implant materials c.p. Ti, Ti–6Al–7Nb and Ti–6Al–4V with different pretreatments. J Mater Sci Mater Med. 1999;10:35–46.
4. Wen HB, Wolke JGC, de Wijn JR, Liu Q, Cui FZ, de Groot K. Fast precipitation of calcium phosphate layers on titanium induced by simple chemical treatments. Biomaterials. 1997;22:1471–8.
5. Sun J, Han Y, Cui K. Microstructure and apatite-forming ability of the MAO-treated porous titanium. Surf Coat Technol. 2008;202:4248–56.
6. Haddow DB, Kothari S, James PF, Short RD, Hatton PV, van Noort R. Synthetic implant surfaces. 1. The formation and characterization of sol-gel titania films. Biomaterials. 1996;17:501–7.
7. Halary-Wagner E, Wagner FR, Brioude A, Mugnier J, Hoffmann P. Light-induced CVD of titanium dioxide thin films II: thin film crystallinity. Chem Vap Depos. 2005;11:29–37.
8. Shtansky DV, Gloushankova NA, Bashova IA, Petrzhik MI, Sheveiko AN, Kiryukhantsev-Korneev FV, Reshetov IV, Grigoryan AS, Levashov EA. Multifunctional biocompatible nanostructured coatings for load-bearing implants. Surf Coat Technol. 2006;201:4111–8.
9. Kweh SWK, Khor KA, Cheang P. An in vitro investigation of plasma sprayed hydroxyapatite (HA) coatings produced with flame-spheroidized feedstock. Biomaterials. 2002;23:775–85.
10. Braceras I, Alava JI, Goikoetxea L, de Maetzu MA, Onate JI. Interaction of engineered surfaces with the living world: ion implantation vs. osseointegration. Surf Coat Technol. 2007;201:8091–8.
11. Garcia-Alonso MC, Saldan L, Valles G, Gonzalez-Carrasco JL, Gonzalez-Cabrero J, Martinez ME, Gil-Garay E, Munuera L. In vitro corrosion behavior and osteoblast response of thermally oxidized Ti6Al4V alloy. Biomaterials. 2003;24:19–26.
12. Chung SH, Heo SJ, Koak JY, Kim SK, Lee JB, Han JS, Han CH, Rhyu IC, Lee SJ. Effects of implant geometry and surface treatment on osseointegration after functional loading: a dog study. J Oral Rehabil. 2008;35:229–36.
13. Kim YH, Koak JY, Chang IT, Wennerberg A, Heo SJ. A histomorphometric analysis of the effects of various surface treatment methods on osseointegration. Int J Oral Maxillofac Implants. 2003;18:349–56.
14. Yamamoto O, Alvarez K, Kikuchi T, Fukuda M. Fabrication and characterization of oxygen-diffused titanium for biomedical applications. Acta Biomater. 2009;5:3605–15.
15. Juopperi TA, Schuler W, Yuan X, Collector MI, Dang CV, Sharkis SJ. Isolation of bone marrow-derived stem cells using density-gradient separation. Exp Hematol. 2007;35:335–41.
16. Mossmann T. Rapid colorimetric assay for cellular growth and survival: application to proliferation and cytotoxicity assays. J Immunol Methods. 1983;65:55–63.
17. Gillies RJ, Didier N, Denton M. Determination of cell number in monolayer cultures. Anal Biochem. 1986;159:109–13.
18. Coelho MJ, Fernandes MH. Human bone cell cultures in biocompatibility testing. Part II: effect of ascorbic acid, β-glycerophosphate and dexamethasone on osteoblastic differentiation. Biomaterials. 2000;21:1095–102.
19. Delhaes P, Couzi M, Trinquecoste M, Dentzer J, Hamidou H, Vix-Guterl C. A comparison between Raman spectroscopy and surface characterizations of multiwall carbon nanotubes. Carbon. 2006;44:3005–13.
20. López-Honorato E, Meadows PJ, Shatwell RA, Xiao P. Characterization of the anisotropy of pyrolytic carbon by Raman spectroscopy. Carbon. 2010;48:881–90.
21. Larouche N, Stansfield BL. Classifying nanostructured carbons using graphitic indices derived from Raman spectra. Carbon. 2010;48:620–9.
22. Goto A, Kyotani M, Tsugawa K, Piao G, Akagi K, Yamaguchi C, et al. Nanostructures of pyrolytic carbon from a polyacetylene thin film. Carbon. 2003;41:131–8.
23. Vallerot JM, Bourrat X, Mouchon A, Chollon G. Quantitative structural and textural assessment of laminar pyrocarbons through Raman spectroscopy, electron diffraction and few other techniques. Carbon. 2006;44:1833–44.
24. Tuinstra F, Koenig JL. Raman spectrum of graphite. J Chem Phys. 1970;53:1126–30.
25. Lian JB, Stein GS. Concepts of osteoblast growth and differentiation-basis for modulation of bone cell-development and tissue formation. Crit Rev Oral Biol Med. 1992;3:269–305.
26. Bellows CG, Aubin JE, Heersche JNM. Initiation and progression of mineralization of bone nodules formed in vitro: the role of alkaline phosphatase and organic phosphate. Bone Miner. 1991;14:27–40.
27. Anderson HC, Morris DC. Mineralization. Physiology and pharmacology of bone. In: Mundy GR, Martin TJ, editors. Handbook of experimental pharmacology. New York: Springer-Verlag; 1993. p. 267–98.
28. Bellows CG, Heersche JN, Aubin JE. Determination of the capacity for proliferation and differentiation of osteoprogenitor cells in the presence and absence of dexamethasone. Dev Biol. 1990;140:132–8.
29. Declercq HA, Verbeeck RMH, De Ridder LIFJM, Schacht EH, Cornelissen MJ. Calcification as an indicator of osteoinductive capacity of biomaterials in osteoblastic cell cultures. Biomaterials. 2005;26:4964–74.
30. Gregory CA, Gunn WG, Peister A, Prockop DJ. An alizarin red-based assay of mineralization by adherent cells in culture: comparison with cetylpyridinium chloride extraction. Anal Biochem. 2004;329:77–84.
31. Lievremont M, Potus J, Guillou B. Use of alizarin red S for histochemical staining of Ca^{2+} in the mouse; some parameters of the chemical reaction in vitro. Acta Anatom. 1982;114:268–80.
32. Ferraz MP, Fernandes MH, Trigo Cabral A, Santos JD, Monteiro FJ. In vitro growth and differentiation of osteoblast-like human bone marrow cells on glass reinforced hydroxyapatite plasma-sprayed coatings. J Mater Sci Mater Med. 1999;10:567–76.
33. Keller JC, Stanford CM, Wightman JP, Draughn RA, Zaharias R. Characterization of titanium implant surfaces III. J Biomed Mater Res. 1994;28:939–46.
34. Bowers KT, Keller JC, Randolph BA, Wick DG, Michaels CM. Optimization of surface micromorphology for enhanced osteoblast responses in vitro. Int J Oral Maxillofac Implants. 1992;7:302–10.

35. Martin JY, Schwartz Z, Hummert TW, Schraub DM, Simpson J, Lankford J Jr, Dean DD, Cochran DL, Boyan BD. Effect of titanium surface roughness on proliferation, differentiation and protein synthesis of human osteoblast-like cells (MG63). J Biomed Mater Res. 1995;29:389–401.
36. Shapira L, Halabi A. Behavior of two osteoblast-like cell lines cultured on machined or rough titanium surfaces. Clin Oral Impl Res. 2009;20:50–5.
37. Boyan BD, Lincks J, Lohmann CH, Sylvia VL, Cochran KL, Blanchard CR, Dean DD, Schwart Z. Effect of surface roughness and composition on costochondral chondrocytes is dependent on cell maturation state. J Orthop Res. 1999;17:446–57.
38. Cochran DL, Simpson J, Weber HP, Buser D. Attachment and growth of periodontal cells on smooth and rough titanium. Int J Oral Maxillofac Implants. 1994;9:289–97.
39. Weiss RE, Reddi AH. Appearance of fibronectin during the differentiation of cartilage bone and bone marrow. J Cell Biol. 1981;88:630–6.
40. Pearson BS, Klebe RJ, Boyan BD, Moskowicz D. Comments on the clinical application of fibronectin in dentistry. J Dent Res. 1988;67:515–7.
41. Bigerelle M, Anselme K, Noël N, Ruderman I, Hardoiun P, Iost A. Improvement in the morphology of Ti-based surfaces: a new process to increase in vitro human osteoblast response. Biomaterials. 2002;23:1563–77.